

Confirmed short periodic variability of subparsec supermassive binary black hole candidate Mrk 231

Andjelka B. Kovačević,^{1*} Tignfeng Yi,² Xinyu Dai,³ Xing Yang,² Iva Čvorović-Hajdinjak
and Luka Č. Popović^{1,4}

¹*Department of astronomy, Faculty of Mathematics, University of Belgrade, Studentski trg 16, 11000, Belgrade, Serbia*

²*Key Laboratory of Colleges and Universities in Yunnan Province for High-energy Astrophysics, Department of Physics, Yunnan Normal University, Kunming 650500, China*

³*Homer L. Dodge Department of Physics and Astronomy, University of Oklahoma, Norman, OK 73019, USA*

⁴*Astronomical observatory Belgrade, Volgina 7, P.O.Box 74 11060, Belgrade, 11060, Serbia*

Accepted XXX. Received YYY; in original form ZZZ

ABSTRACT

Here we confirm the short periodic variability of a subparsec supermassive binary black hole (SMBBH) candidate Mrk 231 in the extended optical photometric data set collected by the Catalina Real-Time Transient Survey (CRTS) and All-Sky Automated Survey for Supernovae (ASAS-SN). Using the Lomb-Scargle periodogram and 2DHybrid method, we detected the significant periodicity of ~ 1.1 yr beyond a damped random walk model in the CRTS+ASAS-SN optical data set. Mrk 231 has been previously proposed as a SMBBH candidate with a highly unequal mass ratio ($q \sim 0.03$), very tight mutual separation of ~ 590 AU, and an orbital period of ~ 1.2 yr. Hence, our result further supports, even though not prove, the intriguing hypothesis that SMBBHs with low mass ratios may be more common than close-equal mass SMBBHs. This result, however, was obtained from the contribution of CRTS data with limited sampling cadence and photometric accuracy, and further monitoring of Mrk 231 is crucial to confirm the periodicity.

Key words: galaxies: active – quasars: supermassive black holes – quasars: individual: Mrk 231

1 INTRODUCTION

Close, gravitationally bound supermassive binary black holes (SMBBHs) are theoretically predicted a long time ago as a consequence of the galaxy mergers (Begelman et al. 1980). As galaxy mergers should be frequent with the expectation that SMBBHs linger at very close mutual distance (Haehnelt & Kauffmann 2002), it is believed that sub-parsec SMBBHs should be common, despite the lack of observational conformations. Now, these intriguing objects are the prominent targets for imminent gravitational wave surveys. Recently, Goulding et al. (2019) reported the discovery of a $z \sim 0.2$ quasar residing in a merger remnant with two closely separated (~ 430 pc) continuum cores at the center of the galaxy SDSSJ1010+1413. These two cores are spatially matched with two powerful [OIII]-emitting point sources with luminosities $\sim 5 \times 10^{46} \text{ergs}^{-1}$, indicating a bound SMBBH system (each object in the pair with $4 \times 10^8 M_{\odot}$).

This finding gives strong support that detection of such systems is possible in the gravitational wave domain. Still, most SMBBHs angular sizes are well below the resolution of direct imaging methods and some other indirect methods are used to detect sub-pc SMBBHs presumably from spectroscopic line shapes and time variability of long term monitored continuum and emission lines (see e. g. Boroson and Lauer 2009; Bon et al. 2012; Graham et al. 2015a,b; Li et al. 2016). Yet as more measurements and analyses have accumulated, that spectral line shapes can not be uniquely coupled to a spatial model of the SMBBHs, the line shape method has seemed increasingly inadequate to use alone (see simulations in Mangham et al. 2019; Kovačević et al. 2019b).

With the development of time domain astronomy, the identification of SMBBHs via periodic variability of light curves hold some promises (see e.g. Haiman et al. 2009; Sesana et al. 2018). This working hypothesis is based on the theoretical prediction that if gas accretion occurs in SMBBH, the orbital period could be imprinted into periodic variability of the continuum and emission lines.

* E-mail: andjelka@matf.bg.ac.rs (ABK)

Proposed spectroscopic SMBBH signatures (e.g. double-peaked profiles) have been identified in large galaxy monitoring samples (Eracleous et al. 2012; Graham et al. 2015a). Even though the results are encouraging, still there are alternate physical explanations for such emission (see e.g. Popović 2012).

Also, the statistical significance of the detected periodic signals is strongly influenced by the underlying stochastic quasar variability and quality of data time coverage. Vaughan et al. (2016) have recently shown that Gaussian red noise models can naturally mimic periodic signals, especially at inferred periods comparable to the length of the observed light curves. Moreover, optical surveys are expected to detect SMBBHs at larger periods where they stay for the largest fraction of their lifetimes (see further discussion in Sesana et al. 2018).

Thus, most binary SMBBH candidates require confirmation with newly available data and newly devised methods for period detection. Upcoming synoptic instruments like LSST will potentially identify hundreds to thousands of such candidates (Shemmer et al. 2018), thus emphasizing the need for new, and effective methods for period detection. From the other side, it is expected that the Event Horizon Telescope (Akiyama et al. 2019) can spatially resolve sub-pc SMBBH, and such confirmations will not be limited by the periodicity detection method or by a condition that source orbital period should be much larger than the monitoring program.

Recently, Yan et al. (2015) proposed an interesting SMBBH candidate (with a very short orbital period) in the nucleus of the nearest quasar Mrk 231 at redshift $z = 0.0422$, based on detailed analysis of its unique optical-UV spectrum. Mrk 231 is the nearest quasar and the most luminous Ultra-Luminous InfraRed Galaxy in the nearby Universe (Feruglio et al. 2010). Lately, the emission feature in its spectra has been reported as the first detection of extragalactic molecular oxygen (Wang et al. 2020). Even the optical spectrum of Mrk 231 resembles mostly the quasar composite spectrum, it varies dramatically at the wavelengths around 3000 Å and becomes flat again at < 2500 Å. They interpreted this unique spectrum of Mrk 231 as a consequence of emission from a BBH accretion system, with which the drop of the continuum at < 4000 Å is due to a gap or a hole opened by the secondary component of the BBH (Gültekin and Miller 2012). The masses of the primary and the secondary SMBBHs were constrained as $\sim 1.5 \times 10^8 M_{\odot}$ and $4.5 \times 10^6 M_{\odot}$, respectively. The semimajor axis of the system is estimated ~ 590 AU, and its orbital period is just ~ 1.2 years, where the corresponding gravitational wave emission would be on tens of nanohertz. If such periodicity could be confirmed from timing observations, this object might be a target for the next generation of gravitational wave detections.

The existence of short time scale periodic signals have been reported in the optical domain for some other active galactic nuclei (AGN). Sandrinelli et al. (2014, 2016) confirmed 315 day period in the light curve of PKS 2155-304 detected previously by Zhang et al. (2014), and also found marginally significant (3σ) periods in PKS 0537-441, OJ 287, 3C 279, PKS 1510-089 and PKS 2005-489, on timescales ranging from dozens of days up to a few years (some of them in harmonic relations). Also, Sandrinelli et al. (2016) found

a marginally-significant (3σ) signal in the optical light curve of OJ 287 with a period of 435 days, in addition to a much less significant one of 203 days.

Having in mind a prior model prediction of a short periodic signal in Mrk 231 and SMBBH model evaluation is an iterative process, we analyze the combined CRTS and ASAS-SN light curves of Mrk 231. Our analysis and extracted results are obtained from for the first time presented 13 year long optical light curve of Mrk 231, utilizing the traditional Lomb-Scargle Periodogram, and the newly introduced 2DHybrid method. We estimate the statistical significance of the identified signal by generating synthetic light curves that show red noise without any periodic signal. This paper is organized as follows. We present, for the first time, combined photometric Mrk 231 light curve in Section 2 and used in Section 3 for periodicity analysis. The main results are summarized in Section 4.

2 OBSERVATIONS

The data sets, we used for the analysis, consist of the V-band light curves obtained by CRTS and ASAS-SN surveys. The data of the V-band light curve of Mrk 231 was taken from The Catalina Surveys Data Release 2 (CSDR2) (Drake et al. 2009, 2013; Graham et al. 2015a). The light curve of the CSRT DR2 V-band contains 113 epochs data collected between May 2005 and June 2013. The effective wavelength of the V-band is 5510 Å.

The ASAS-SN V-band data were recorded by the Brutus (Haleakala, Hawaii) and Cassius (CTIO, Chile) quadruple telescopes between 2013 and 2018. ASAS-SN V-band field is observed to a depth of $V \lesssim 17$ mag. The field of view of an ASAS-SN camera is 4.5 deg^2 , the pixel scale is $8''0$ and the FWHM is typically ~ 2 pixels. The ASAS-SN V-band light curves were processed via method explained in Jayasinghe et al. (2018) using image subtraction (Alard and Lupton 1998; Alard 2019) and aperture photometry on the subtracted images with a 2-pixel radius aperture. The APASS catalog (Henden et al. 2015) was used for calibration. We corrected the zero point offsets between the different cameras as described in Jayasinghe et al. (2018). The photometric errors were estimated as prescribed by Jayasinghe et al. (2019).

However, due to differences in the wavelength response of telescopes, and zero- point calibration systematic offsets between light curves from CRTS and ASAS-SN telescopes can be present. We tested for these offsets by calculating the differences between the average values of the two light curves. The mean magnitude of CRTS and ASAS-SN data are 12.952 and 13.256 respectively, so the difference between them is 0.304. We let the CRTS data to be translated for 0.304 magnitudes to be consistent with the ASAS-SN data (see Fig. 1). We applied these calculated shifts of the mean values of two light curves to produce the combined light curve (see Table 1). Table 1 is available in the electronic supplementary material.

In Table 2 we show some characteristic parameters of the combined CRTS and ASAS-SN light curves. This shows that the ASAS-SN part of the light curve is more variable than the CRTS part, thus contributing more to the variability of the combined curve. CRTS part of the light curve

Table 1. The combined V band light curve of Mrk 231. The columns display Modified Julian Date, magnitude and magnitude uncertainties, respectively. Complete data are available online.

MJD	mag	σ
53505.21965	13.034	0.06
53767.31269	13.214	0.05
53767.31765	13.204	0.05
53767.32261	13.214	0.05
53767.32757	13.214	0.05
53860.36368	13.244	0.05
53860.37032	13.264	0.05
53860.37695	13.254	0.05
53860.38362	13.244	0.05
53884.24010	13.274	0.05
53767.32261	13.214	0.05
...

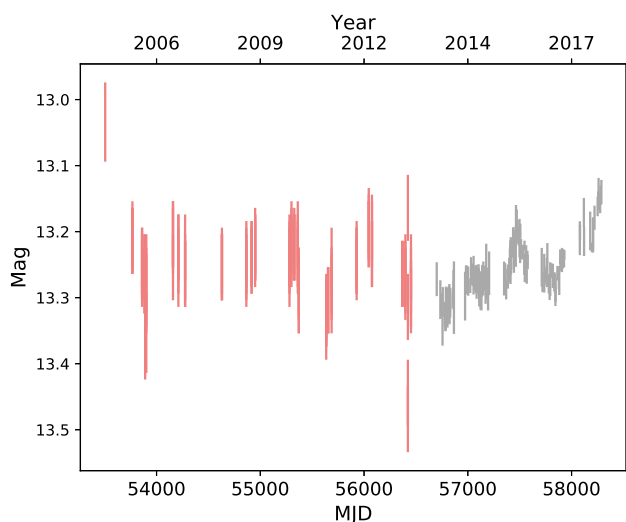


Figure 1. The combined long-term V band light curve of Mrk 231. This consists of CRTS (red error bars, MJD<56500) and ASAS-SN (black errorbars, MJD>56500) data points. To create the combined record we use magnitude difference $\delta m = 0.304$. The errorbars stand for 1σ standard deviation of the measurement. Time is given as Modified Julian days (MJD).

is almost three times less variable than the ASAS-SN part. Moreover, the ASAS-SN mean sampling rate is almost three times better than CRTS. Also, CRTS data is more sparse with larger season gaps, and ASAS-SN data is denser with smaller time gaps. As a summary, these characteristics might negatively influence the quality of results based on the CRTS data set.

3 METHODS OF PERIODICITY DETECTION IN THE LIGHT CURVES

There are many characteristics of the astronomical observations, which severely complicate period analyses: the limited length of the light curves, the presence of gaps in the light curves (e.g., seasonal observing opportunities, seeing, etc.) and uneven sampling as well. Extended gaps in time series

are difficult because their duration can be comparable to the duration of the observations in a year. This problem is evident in the optical light curve of Mrk 231 (Fig. 1). For this purpose, we applied two different procedures for periodicity detection which are briefly outlined below.

3.1 Lomb-Scargle periodogram

An extension of the Fourier technique that attempts to circumvent above mentioned limitations is the Lomb-Scargle periodogram (LSP Lomb 1976; Scargle 1982). The LSP is the most widely used statistical tool for detecting periodic signals in unevenly-spaced observations in the last few decades. It utilizes correction of the functional basis of the Fourier transform to sustain normalization condition on an uneven grid of time instances of observation. The prominent attributes of the Lomb-Scargle normalized periodogram are avoidance of the interpolation of missing data and a per-point rather than a per-time-interval weighting observations (Frick et al. 1997).

We used the LSP implementation in astropy package of Python. For a detailed practical discussion of LSP based on astropy see Vanderplas (2018). Some odd characteristics of LSP has been noted. The LSP can be sensitive to frequencies higher than the average Nyquist frequency. The periodogram can have many spurious peaks, which can arise due to several factors. For example, when the signal is not a perfect sinusoid, additional peaks can appear indicating higher-frequency components in the signal. Uncertainties in observations could cause loss of power from the true peaks. Also, the LSP method is based on a least square regression and, its results can be reactive to outliers in the light curve. The consequence of these effects means that the highest LSP peak may not correspond to the most probable frequency, and the analysis results must be interpreted carefully (see discussion in Vanderplas 2018).

The calculated LSP of the optical light curve in the V band is presented in Fig 2 and in Table 2, which clearly shows 3 peaks of similar amplitude and width. These three peaks are very close to each other: 195 days, 265 days and 416 days (1.13 yr). The difference between the first two peaks is 70 days (or about two months), which is not related to the sampling patterns of the curves (see Table 2). The uncertainties are obtained as the Full-widths at half-maxima (FWHM) of Gaussian fits to the corresponding periodogram peaks.

3.2 2DHybrid method

Although the LSP method accounts for irregular spacing in a time series, the method assumes sinusoidal forms of the underlying signal and does not take into account time fluctuations in the periodic signal information. In real astronomical systems, oscillations can be damped or deformed. In such cases, the wavelet transform method proves to be a more useful tool, and it is often applied in the analysis of blazar sources (see e. g. Bhatta et al. 2013; Hovatta et al. 2000).

The innovative algorithm for extraction of periodic signals, 2DHybrid, can robustly distinguish between pure stochastic red noise and a mixture of red noise plus periodic

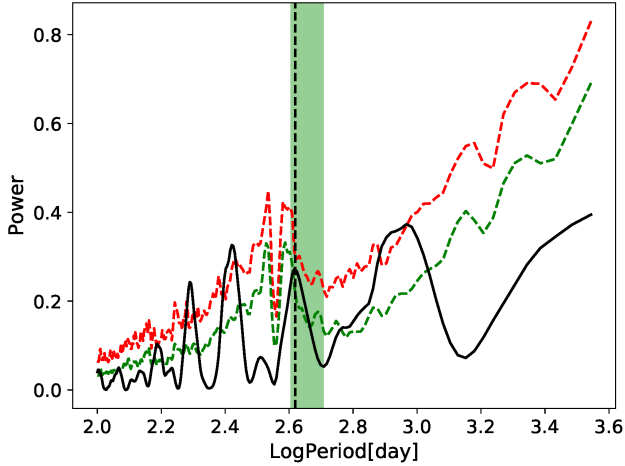


Figure 2. The LSP computed from the photometric light curve of Mrk231 (black) shown in Fig. 1, and the corresponding 95% and 99.7% confidence curves (green (lower) and red (upper) dashed line), for a red noise spectrum with $\alpha = 1.85$ (see Subsection 3.3). The vertical dashed line denotes the period of 416 days. The green shaded region indicates a range for Yan et al (2015) periodicity prediction, which is $1.2^{+0.2}_{-0.1}$ yr.

signal in AGN light curves (Kovačević et al. 2018, 2019a). In the interest of completeness, we briefly summarize the method here. Simply knowing the continuous wavelet transform matrix (\mathcal{T}_i) of the light curve (c_i), we estimate the envelope of present signals $\mathcal{E}_i = \sqrt{\mathcal{T}_i \cdot \mathcal{T}_i}$, where operations are on complex matrices. Then we correlate the envelopes of the light curves (c_i, c_j) as follows $\mathcal{R} = \text{corr}(\mathcal{E}_i, \mathcal{E}_j)$. In the case of Mrk 231, we have only one curve, and all formulas are used for $i = j$. The 2DHybrid method is general and different from other methods (such as LSP) since it does not assume any form of signal and its principles are similar to 2D spectroscopy. Instead of the typical 1D representation of frequencies, 2DHybrid method extends the search for signals in 2D, quantifying the strength of the interaction between oscillations in different light curves as well as the level of the autocorrelation of signals in a single curve, which is important in classification of different physical origin of AGN variability. For example, besides periodic oscillations typical e. g. SMBBH candidates, the 2DHybrid allows classification of other types of objects according to fluctuations of oscillations in 2D (auto)correlation space.

The 2DHybrid method results (see Figure 3 and Table 2) indicate that the correlation intensity for the characteristic periods centered at 403 days is highly significant (larger than 99.7%), which is similar to the LSP result of period 413 days with significance larger than 95%. Their uncertainties are evaluated as the means of the FWHMs of the Gaussian fits centered around the peaks at a given period. The relatively larger uncertainty in the 2DHybrid-derived periods mainly arises from the temporal variation of the periodicities. The average oscillation power is quite similar to the LSP power.

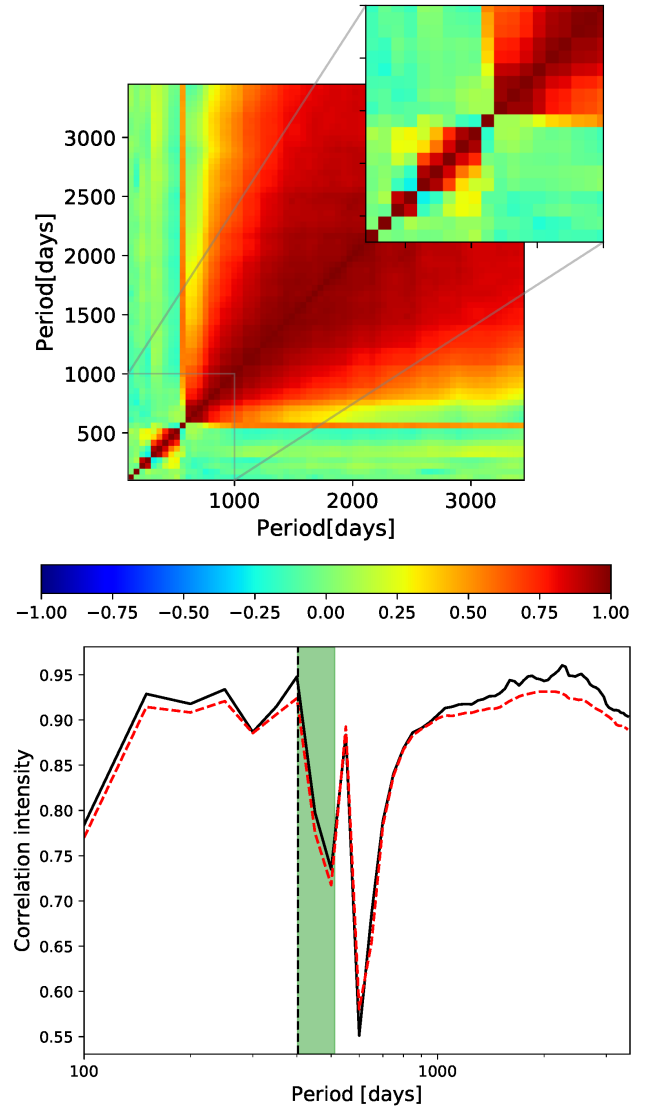


Figure 3. Upper panel: The color-scaled correlation intensity (red for high correlation intensities) of coupling of periods in the combined light curve of Mrk 231 in the period-period plane. Three prominent periods are present in red in the lower-left corner ($\sim 195, \sim 265$ and ~ 403 days, from left to the right). Correlation islands (~ 0.25) indicate an asynchronous coupling between different periods. Inset: zoomed region in period-period plane between 100 and 1000 days, where three periods are seen. Lower panel: Time averaged 2DHybrid correlation intensity as a function of the period (solid black curve), and 99.7% confidence curve (red dashed-line) from the simulation. The vertical dashed line marks the period of 403 days (1.1 yr). The green shaded region indicates a range for Yan et al (2015) periodicity prediction, which is $1.2^{+0.2}_{-0.1}$ yr.

3.3 Estimation of red noise effects

As already mentioned, the effects of uneven sampling of a light curve can produce spurious peaks in the periodogram that can be mistaken for a real signal. Moreover, the LSP and 2DHybrid methods in Mrk 231 light curve, we take into account both the uneven sampling including seasons gaps of the object light curve and the red noise. To do so, we

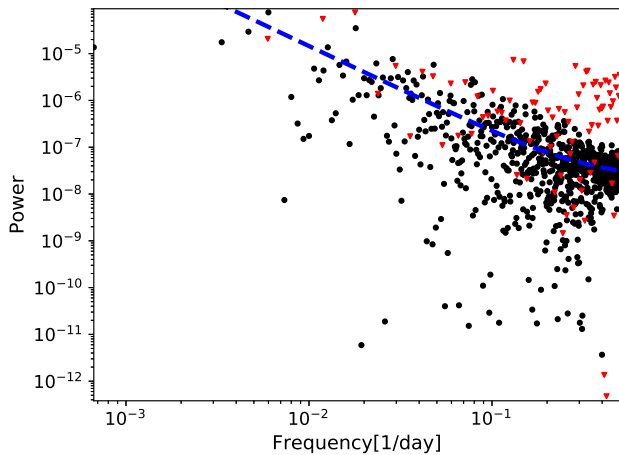


Figure 4. PSD of artificially upsampled ASAS-SN part of Mrk 231 light curve (black dots). The best fit model (blue dashed line) has a spectral power-law index 1.85 and break frequency 0.0005 days^{-1} . Red down triangles mark PSD of original data obtained using the LSP method from the Python module *astropy*.

simulate one thousand red-noise light curves of the source, obtained based on [Timmer & Koenig \(1995\)](#) method.

First, as an input parameter for simulating the red noise light curves, we calculate the power law index of the underlying red noise of the source. We used a broken power-law of the form $P(\nu) \sim [1 + (\nu/\nu_b)^2]^{-\alpha}$ where α and ν_b stand for the spectral slope and the break frequency, respectively. This, so-called damped random walk ($\alpha = 2$) is widely used to model optical light curves of AGN.

Fitting was based on the adapted Basin-hopping of a stochastic algorithm (see theory in [Emmanoulopoulos et al. 2013](#); [Connolly 2016](#), and for pythonic implementation) which attempts to find the global minimum of a given function. As a consistency check, the algorithm can be run from a number of different random starting points so that the process of calculation converges to the global minimum. One thousand iterations of the Basin-Hopping algorithm is carried out. Each iteration restarts the minimization from a different value, in order to ensure that the actual minimum is found. The resulting best-fit model, corresponding to $\nu_b^{-1} = 2000$ days and $\alpha = 1.85$, is shown as the dashed blue line in Fig. 4.

For this procedure, we upsampled the original non-uniformly sampled data by fitting Gaussian process (GP) with Ornstein Uhlenbeck kernel ([Kovačević et al. 2018](#)) aka Damped random walk (DRW). This kernel has been widely used in quasar light curve modeling ([Kelly et al. 2009](#); [MacLeod et al. 2010](#); [Kozłowski et al. 2010](#)). For seeing the effects of this upsampling, we calculate power spectral density function (PSD) of the original data using the LSP method in the *astropy* module of Python (see Fig. 4). There are two dozens of original data points (out of 200) that are in subregion parallel to the PSD obtained from GP upsampled curve. The consequence of this fitting and interpolation procedure is that in the same bandwidth as for the original data, the interpolated data set has a decreased dispersion.

The best-fit PSD was used to generate 1000 artificial light curves of Mrk 231, which has the same sampling, stan-

dard deviation and mean as the observed light curve. We analyse obtained distribution of this artificial light curves to infer the significance of the peaks seen in the observed LSP. We calculate 95% and 99.7% (or $\sim 3\sigma$) statistical significance curve as the 95th and 99.7th percentile of distribution of the power in the LSP (see Fig. 2 of the simulated light curves).

Similarly, we calculate the significance of the observed correlation intensity of the light curve using the 2DHybrid method applied on the 1,000 simulated light curves from the previously described PSD model, and their distribution of correlation intensity calculated in the period-period phase space (alternatively it can be calculated in frequency-frequency space). The observed correlation intensity was compared with 99.7% confidence level (as the 99.7th percentile at a given period) from the distribution of the averaged correlation intensity for the simulated light curves given in Fig. (3). The significance of the peak centered at 403 days is above 99.7%. This approach of peaks significance determination is similar to that proposed by [Vaughan \(2005\)](#) for evenly sampled data, but modified here by using the LSP and 2DHybrid method instead of the Fourier transform.

3.4 Analysis of CRTS and ASAS-SN parts of the light curve

Previous analyses in Subsections 3.1-3.2 were carried out on the whole data set. Here we examined CRTS and ASAS-SN data sets separately in the same manner as in the case for the combined light curve.

The CRTS part of the light curve shows a period of 609 days in LSP analysis which is above 95% significance but lower than 99.7% (see upper panel Fig. 5). The 2DHybrid method indicates the presence of a signal of 441 days above 99.7% (see bottom panel Fig. 5). The ASAS-SN part of the curve exhibits the period of 420 days from LSP analysis, which is barely above 95% but lower than 99.7% (see upper panel Fig. 6). However, the 2DHybrid method detected a strong signal at 479 days, above 99.7% significance. Based on these results, the ASAS-SN observations have a large influence on the LSP, which is expected due to the smaller uncertainties. The confidence contours of the 2DHybrid method in certain parts are almost indistinguishable from the correlation intensity of the observed curve in the scales of corresponding figures, as their values are rather close.

4 DISCUSSION AND CONCLUSIONS

For mass ratios $q > 0.05$, hydrodynamical simulations indicate that commensurability patterns should be present among oscillations in the light curves of binaries ([D’Orazio et al. 2015](#)). The periodogram peaks can appear as commensurability of orbital periods of components 1/2, as well as in commensurability of hotspot period, orbital period and half of the orbital period of the binary (from 1/3/6 to 1/8/16 see in [Charisi et al. 2015](#)). In our calculations, both LSP and 2DHybrid methods detected three peaks in analysis of combined curve. The peaks at 195 and 403 days are roughly commensurable. The third peak of 265 days is not commensurable with the other two, but it is in rough 3/5 commensu-

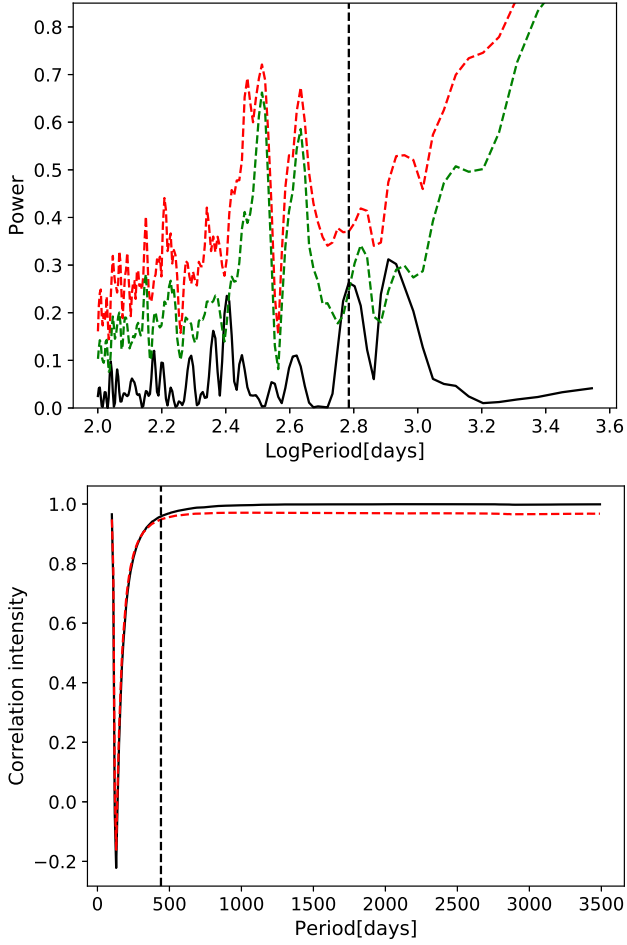


Figure 5. Periodicity analysis of CRTS part of the light curve. Upper panel: LSP analysis, the vertical dashed line indicates a period of 609 days. The green (lower dashed) and red (upper dashed) curve indicate 95% and 99.7% significance, while the solid black curve is the measured curve. Lower panel: Hybrid analysis, the vertical dashed line indicates a period of 441 days. The red dashed curve indicates 99.7% significance, while the black solid curve is the measured curve.

reability with peak of 403 days. This peak cannot be a consequence SMBBH orbital dynamics; however, it can arise due to some other processes either in circumbinary disk or in disks of components. Yan et al. (2015) interpreted the UV spectral signature of Mrk 231 as a consequence of emission from a circumbinary disc with a central cavity, dynamically opened by the secondary SMBH. But for low mass ratios as it is assumed to be in the case of Mrk 231, a cavity may not be present as suggested by D’Orazio et al. (2016); Farris et al. (2016). Leighly et al. (2016) suggested that the UV emission of Mrk 231 is more likely to be consistent with a reddened AGN with a special extinction law. Under this model, the UV emission from the nucleus is completely obscured by the dust and the observed UV flux is interpreted from starburst activities from the host galaxy, which does not forecast variability on short timescales. Yang et al. (2018) analyzed Swift data and detected a significant UV variability of Mrk 231 consistent with accretion disk emission with a characteristic red-noise spectrum. Both, our result and Yan et al.

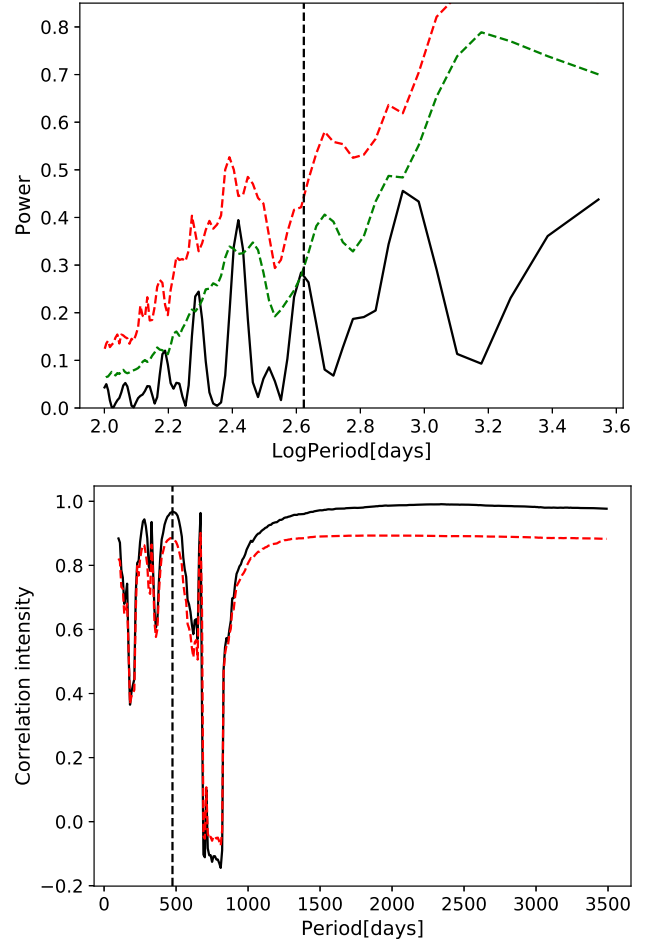


Figure 6. Periodicity analysis of the ASAS-SN part of the light curve. Upper panel: the LSP analysis, the vertical dashed line indicates a period of 420 days. The green (lower dashed) and red (upper dashed) curve indicate 95% and 99.7% significance, while the black solid curve is the measured curve. Bottom panel: 2DHybrid analysis, the vertical dashed line indicates a period of 479 days. The red dashed curve indicates 99.7% significance, while the black solid curve is the measured curve.

(2015) SMBBH model suggest that a possible 1.1 ~1.2 yr periodic variation could be also detected in the UV emission of Mrk 231; however, probing this frequency is beyond the range of current UV data (see Yang et al. 2018). The detailed UV emission location is still uncertain, although it is largely constrained within the central engine, and results of reverberation mapping campaigns can help to identify AGN variability model. For instance, any indication of the UV/optical variations lagging behind the X-ray ones in Mrk 231 emission would support scenario of variability due to reprocessed X-ray emission by the accretion disc (see Yang et al. 2018). The signal of 1.1 yr is always present in our LSP analysis with an almost unaltered amplitude. Previous studies of red noise light curves show that larger LSP peaks are more likely to appear at low frequencies (Meyer et al. 2008), but we do not observe this phenomenon in Mrk 231 light curve. Also, astronomical periodic signals often significantly depart from sinusoids. Thus, the results of the LS periodogram is less optimal compared to 2DHybrid method, since the periodic

variation would be fitted inadequately. This is seen in the light curves of some variable stars and in the radial velocity curves of stars orbited by a planet on an eccentric orbit (see details in Baluev 2009). Also, Lachowicz and Czerny (2005) showed that a simple damped oscillator represents well the time-resolved light-curve properties of Cyg-X1. We use the complex Morlet wavelet, which means that we probe the signal which is deformed in the 2DHybrid analysis.

If the detected periodicity (P) is assumed as the redshifted (z) orbital period of a SMBBH orbital period (O) (Graham et al. 2015b), we can estimate some parameters related to the hypothetical binary system in Mrk 231. As listed in Table 3, we give the orbital period $O = P/(1+z)$; SMBBH mutual distance if the motion is circular

$$r = \left(\frac{GMP^2}{4\pi^2} \right)^{\frac{1}{3}}, \quad (1)$$

where G and M are the gravitational constant and the total mass of the assumed binary system. We also calculate the maximum angular separation if a circular orbit is assumed $\theta = r/D_A$, where D_A stands for the angular size distance in the standard cosmology of a flat universe having Hubble constant $H_0 = 67.8 \text{ km s}^{-1} \text{ Mpc}^{-1}$ and a matter density parameter $\Omega_m = 0.308$ (Planck Collaboration 2016). Finally, we calculate the time of coalescence of SMBBH, namely the time at which, formally, the relative distance due to gravitational waves emission vanishes (Peters 1964):

$$\tau_{GW} = \frac{5}{256} \frac{c^3}{G^3} \frac{r^4}{(M_1 + M_2)M_1M_2}, \quad (2)$$

where M_1 and M_2 are masses of the primary and secondary component, respectively.

Charisi et al. (2016) identified a statistically significant population of 50 periodically variable quasars. These objects show short periods of a few hundred days. Also, they found that the distribution of periods of this population supports SMBBHs with a low mass ratio ($q \sim 0.01$). Although hydrodynamical simulations of SMBBHs with larger mass ratios $q > 0.3$ (e.g. Roedig et al. 2012; Farris et al. 2014) predict that the optical periodicity may not always arise due to the binary orbital period but it can be a consequence of some other superimposing phenomena in binary systems (e.g. lump in the lopsided accretion disc). In general, periodic variability of quasars can also be explained as quasi-periodic modulations arising from surrounding regions of a single SMBH due to Lense-Thirring precession, a warped accretion disc, or the precession of a jet (Graham et al. 2015a).

Interpreting our results in combination with those from other studies of highly unequal mass SMBBH systems (Vanderplas 2012; D’Orazio et al. 2015; Zheng et al. 2016; D’Orazio et al. 2015), invokes the highly unexpected scenario that SMBBHs with low mass ratios may be more frequent than equal mass ratio systems. Our results are also a consequence of the better photometry and the better sampling of the ASAS-SN data compared to the CRTS. In this work, we identified a period of 403 days in the optical light curve of Mrk231. This period obtained from the timing analysis matches Yan et al. (2015) prediction, which strengthens the SMBBH hypothesis.

However, due to the limited photometric accuracy of the data from CRTS, it seems crucial to further follow this object to confirm its periodicity. Also, in other bands such

as UV, Yang et al. (2018) have detected UV variability of Mrk 231. An independent UV periodicity confirmation will further validate the SMBBH nature of Mrk 231.

ACKNOWLEDGEMENTS

This work is supported by Science and Technological development of Republic Serbia through the *Astrophysical Spectroscopy of Extragalactic Objects* project number 176001, and by the National Natural Science Foundation of China (grants 11863007) and the Ministry of Education. XD acknowledges the financial support from NSF grant AST-1413056. ASAS-SN is supported by the Gordon and Betty Moore Foundation through grant GBMF5490 to the Ohio State University, and NSF grants AST-1515927 and AST-1908570. Development of ASAS-SN has been supported by NSF grant AST-0908816, the Mt. Cuba Astronomical Foundation, the Center for Cosmology and AstroParticle Physics at the Ohio State University, the Chinese Academy of Sciences South America Center for Astronomy (CAS- SACA), the Villum Foundation, and George Skestos.

REFERENCES

- Akiyama K., Alberdi A., Alef W., Asada K., Azulay R., et al., 2019, *ApJL*, 875, L6
- Alard C., 2000, *A&AS*, 144, 363
- Alard C., Lupton R. H., 1998, *ApJ*, 503, 325
- Baluev R. V., 2009, *MNRAS*, 395, 1541-1548
- Begelman M. C., Blandford R. D., Rees M. J., 1980, *Nature*, 287, 307
- Bhatta G., Webb J. R., Hollingsworth H., Dhalla S., Khanuja A., Bachev, R. et al., 2013, *A&A*, 558, id.A92, 10
- Borson T. A., Lauer T. R., 2009, *Nature*, 458, 53
- Bon E., Jovanović P., Marziani P., Shapovalova A. I., Bon N., Borka Jovanović V., Borka D., Sulentic J., Popović, L. Č., 2012, *ApJ*, article id. 118, 8
- Charisi M., Bartos I., Haiman Z., Price-Whelan A. M., Márka, S., 2015 *MNRAS*, 454, L21
- Charisi M., Bartos I., Haiman Z., Price-Whelan A. M., Graham M. J. et al., 2016, *MNRAS*, 463, 2145
- Connolly, S. D., 2016, *Astrophysics Source Code Library*
- Drake A. J., Djorgovski S. G., Mahabal A., Beshore E., Larson S., Graham, M. J. et al., 2009, *ApJ*, 696, 870
- Drake A. J., Catelan M., Djorgovski S. G., Torrealba G., Graham M. J. et al, 2013, *ApJ*, 763,32
- D’Orazio D. J., Haiman Z., Schiminovich D., 2015, *Nature*, 525, 351
- D’Orazio D. J., Haiman Z., Duffell P., MacFadyen A. I., Farris B. D., 2016, *MNRAS*, 459, 2379
- Emmanoulopoulos D., McHardy I. M., Papadakis I. E., 2013, *MNRAS*, 433, 907
- Eracleous M., Borson T. A., Halpern J. P., Liu J. 2012, *ApJS*, 201, 23 (21 pp)
- Farris B. D., Duffell P., MacFadyen A. I., Haiman Z., 2014, *ApJ*, 783, 134
- Farris B. D., Duffell P., MacFadyen A. I., Haiman Z., 2015, *MNRAS*, 447, L80
- Feruglio C., Maiolino R., Piconcelli E., et al. 2010, *A&A*, 518, L155
- Frick P., Baliunas S. L., Galyagin D., Sokoloff D., Soon W., 1997, *ApJ*, 483, 426
- Goulding A. D., Pardo, K., Greene, J. E., Mingarelli, C. M. F., Nyland, K., Strauss, M., 2019, *ApJL*, 879, L21

Table 2. Summary of light curve characteristics and detected periods. L , mag_{mean} , σ_{mean} are the total time baseline, mean magnitude and mean magnitude error of the light curves, respectively; N , s_{mean} and s_{median} are the number of data points, mean and median sampling of the light curves; F_{var} is the fractional variability of the light curves; the last four columns provide results for period detection based on LSP and 2DHybrid methods including the significance of the peaks (sig), respectively.

Data	L [days]	mag_{mean}	σ_{mean}	N	s_{mean} [days]	s_{median} [days]	F_{var}	LSP [days]	sig_{LSP} [%]	2DHybrid [days]	$\text{sig}_{2\text{DHyb}}$ [%]
CRTS+ASAS-SN	4782	13.25	0.03	277	17.33	2.98	0.0023	416±34	95	403±29	99.7
CRTS	2947	12.95	0.05	113	26	0.006	0.0011	609± 54	95	441±201	99.7
ASAS-SN	1587	13.26	0.017	164	9.5	3.98	0.0029	413± 40	95	475± 75	99.7

Table 3. SMBBH properties based on a detected period of ~403 days. Columns are described in the text. Masses for primary M_1 and secondary M_2 components are taken from Yan et al. (2015).

M_1 [M_{\odot}]	M_2 [M_{\odot}]	O [days]	r [pc]	θ [μas]	τ_{GW} [yr]
$1.5 \cdot 10^8$	$4.6 \cdot 10^6$	~403	0.00294	3.5	4.1×10^5

- Graham M. J., Djorgovski S. G., Stern D., Drake A. J., Mahabal A. A. et al., 2015a, MNRAS, 453, 1562
- Graham, M. J., Djorgovski G., Stern D., Glikman E., Drake A. et al., 2015b, Nature, 518, 74
- Gültekin K., Miller J. M., 2012, ApJ, 761, id. 90, 6 pp.
- Haehnelt M. G., Kauffmann G., 2002, MNRAS, 336, L61
- Haiman Z., Kocsis, B., Menou K., 2009, ApJ, 700, 1952
- Henden A. A., Levine S., Terrell D., Welch D. L., 2015, American Astronomical Society Meeting Abstracts #225, 336.16
- Hovatta, T., Lehto, H. J., Tornikoski, M., 2008, A&A, 488, 897
- Jayasinghe T., Kochanek C. S., Stanek K. Z., et al., 2018, MNRAS, 477, 3145
- Jayasinghe T., Kochanek C. S., Stanek K. Z., et al., 2019, MNRAS, 485, 961
- Kelly, B. C., Bechtold, J., Siemiginowska, A., 2009, ApJ, 698, 895
- Kochanek, C. S., Shappee, B. J., Stanek, K. Z., et al. 2017, PASP, 129, 104502
- Kovačević A. B., Pérez-Hernández, E., Popović, L. Č., Shapovalova A. I., Kollatschny, W., Ilić D., 2018, MNRAS, 475, 2051
- Kovačević A. B., Popović, L. Č., Šimić S., Ilić D., 2019a, ApJ, 871, id. 32, 11 pp
- Kovačević A. B., Wang, J.-M., Popović, L. Č., 2019b, accepted in A&A, doi.org/10.1051/0004-6361/201936398
- Kozłowski S., Kochanek C. S., Udalski A., Wyrzykowski L., et al., 2010, ApJ, 708, 927
- Lachowicz P., Czerny B., 2005, MNRAS, 361, 645
- Leighly K. M., Terndrup D. M., Gallagher S. C., Lucy A. B., 2016, ApJ, 829, 4
- Li Y.-R., Wang, J.-M., Ho L. C., Lu, K.-X., Q. J., Du P., Hu C. et al., 2016, ApJ, 822, id. 4, 21 pp
- Lomb N. R., 1976, The Astrophysical Journal Supplement Series, 39, 447
- MacLeod C. L., Ivezić Ž., Kochanek C. S., Kozłowski S., Kelly B., Bullock E., et al. 2010, ApJ, 721, 1014
- Mangham S. W., Knigge C., Williams, P., Horne K., Pancoast, A., Matthews J. H et al., 2019, MNRAS, 488, 2780
- Meyer, L., Do, T., Ghez, A., Mark, M. R., Witzel, G. et al., 2008, ApJ, 688, L17
- Peters P. C., 1964, Physical Review, 136, 1224
- Planck Collaboration, Ade, P. A. R., Aghanim N., Arnaud M., Ashdown M., Aumont J. et al., 2016, A&A, 594, A13
- Popović L. Č., 2012, New Astronomy Reviews, 56, 74
- Roedig C., Sesana A., Dotti M., Cuadra J., Amaro-Seoane P., Haardt F., 2012, A&A, 545, A127
- Sandrinelli A., Covino S. Treves A., 2014, ApJL, 793, article id. L1,
- Sandrinelli A., Covino S., Dotti M., Treves A., 2016, ApJ, 151, article id. 54, 14 pp.
- Shemmer O., Richards G., Brandt N., Assef R., Jiang Y.-F., Barth A. et al., 2018, LSST AGN Science Collaboration Roadmap, 25 pp
- Scargle J. D., 1982, The ApJ, 263, 835
- Shappee, B. J., Prieto, J. L., Grupe, D., et al. 2014, ApJ, 788, 48
- Sesana A., Haiman Z., Kocsis B., Kelley, L. Z., 2018, ApJ, 856, id. 42, 14
- Timmer J., Koenig M., 1995, A&A, 300, 707
- Valtonen M. J., Ciprini S., Lehto H. J., 2012, MNRAS, 427, 77
- VanderPlas J. T., 2018, The Astrophysical Journal Supplement Series, 236, pp. 28
- Vaughan, S., 2005, A&A, 431, 391
- Vaughan S., Uttley P., Markowitz A. G., Huppenkothen D., Middleton M. J., Alston W. N., Scargle J. D., Farr W. M., 2016, MNRAS, 461, 3145
- Wang J., Li D., Goldsmith P. F., Zhang, Z.-Y., Gao, Y. et al., 2020, ApJ, 889, 129
- Yan C.-S., Lu Y., Dai X., Yu Q., 2015, ApJ, 809, id. 117, 9 pp
- Yang L., Dai X., Lu Y., Zhu Z.-H., Shankar F., 2018, MNRAS, 480, 5504
- Zhang B.-K., Zhao, X.-Y., Wang C.-X., Dai B.-Z. 2014, Research in astronomy and astrophysics, 14,933
- Zheng Z.-Y., Butler N. R., Shen Y., Jiang L., Wang J.-X., Chen X., Cuadra J., 2016, ApJ, 827, id.56, 10 pp

This paper has been typeset from a $\text{\TeX}/\text{\LaTeX}$ file prepared by the author.